PHYSICAL REVIEW D **93,** 036006 (2016)

Continuum study of the QCD phase diagram through an OPE-modified gluon propagator

Chao Shi,[1,2,4] Yi-Lun Du,[1] Shu-Sheng Xu,[2,4] Xiao-Jun Liu,[1,*] and Hong-Shi Zong[2,3,4,†]

[1]*Key Laboratory of Modern Acoustics, MOE, Institute of Acoustics, and Department of Physics, Collaborative Innovation Center of Advanced Microstructures, Nanjing University, Nanjing 210093, China*

[2]*Department of Physics, Nanjing University, Nanjing 210093, China*

[3]*Joint Center for Particle, Nuclear Physics and Cosmology, Nanjing 210093, China*

[4]*State Key Laboratory of Theoretical Physics, Institute of Theoretical Physics, CAS, Beijing 100190, China*

(Received 9 July 2015; published 18 February 2016)

Within the Dyson-Schwinger equation framework, a gluon propagator model incorporating a quark's feedback through operator product expansion is introduced to investigate the QCD phase diagram in the temperature-chemical-potential ($T-\mu$) plane. Partial restoration of chiral symmetry at zero temperature and finite temperature are both studied, suggesting a first order phase transition point on the μ axis and a critical end point at $(T_E,\mu_E)/T_c=(0.85,1.11)$, where T_c is the pseudocritical temperature. In addition, we find the pseudocritical line can be well parametrized with the curvature parameter κ and a consistent decrease in κ, with more of the gluon propagator distributed to the quark's feedback.

DOI: 10.1103/PhysRevD.93.036006

I. INTRODUCTION

The Universe went through a quark epoch approximately 10^{-12} seconds after the big bang. Nowadays, the nucleus-nucleus collisions at the RHIC and the LHC with a high center of mass energy can reproduce a state known as the quark-gluon plasma (QGP) [1,2]. It consists of unbound quarks/gluons and behaves as a nearly perfect fluid [3,4] with very small viscosity. While progress is being made in studying the QGP concerning the high temperature (T) and low chemical-potential (μ) region in the QCD phase diagram, little is known about the territory with a higher μ. Hence, the RHIC is planning a beam energy scan program phase II (BES II) based on the BES I completed in 2014 [5,6]. With statistical errors largely reduced, strong conclusions on QCD phase transition boundary and the critical end point (CEP) are hopefully to be drawn.

On the theoretical side, with finer lattices and physical quark masses, lattice simulations observed the analytical crossover behavior at $T\neq 0,\mu=0$ and investigated various thermodynamic quantities of the QGP [7–9]. However, its extrapolation to $\mu\neq 0$ is a yet unsolved problem due to the notorious sign problem [10–12]. Therefore, alternative approaches to the QCD phase diagram like (Polyakov–) Nambu–Jona-Lasinio [(P)NJL] models [13,14], quark-meson models [15–17], and the Dyson-Schwinger equation (DSE) method [18–21] could provide valuable insights at present [22].

In this work, we will resort to DSEs, which is a continuous nonperturbative approach that describes QCD's several important features, e.g., dynamical chiral symmetry breaking (DCSB) and confinement [23]. It has been employed in extensive study on the QCD phase diagram. For instance, chiral phase restoration was studied over the $T-\mu$ space and, generally speaking, the existence of the CEP is suggested, consistent with most model predictions. It is further supplemented by the investigation of certain phases, e.g., strongly interacting QGP at high temperature [24,25] and color superconductivity at low temperature [26]. The effect of chiral imbalance on the QCD phase structure is also studied, extending the phase diagram to $T-\mu-\mu_5$ space [27,28].

As an infinite tower of equations, DSEs always require truncation schemes, in practice. For example, the quark's DSE, namely, the quark gap equation, has two unknown ingredients: the quark-gluon vertex and the gluon propagator. For the quark-gluon vertex, commonly used are the following. (i) Rainbow truncation, namely, the bare vertex which had been widely used in combination with the ladder truncation in bound state problems. (ii) The Ball-Chiu ansatz [29] and its modified versions that concern the Abelian and non-Abelian dressing effects [30]. (iii) The Ball-Chiu ansatz plus a dressed-quark anomalous chromomagnetic moment term [24]. In spite of the fact that the latter two vertices are more refined, rainbow truncation suffices to give qualitative descriptions of the QCD phase diagram in almost all aspects. Therefore, we will use it throughout this work for simplicity.

With rainbow truncation, our main focus in the work will be on the other ingredient of the quark self-energy, the gluon propagator. A popular choice is to directly generalize models determined in hadron physics, e.g., a separable model [31,32], the Maris-Tandy model [33], the Qin-Chang

*liuxiaojun@nju.edu.cn
†zonghs@nju.edu.cn

model [34], etc.,[1] to the finite temperature case [18,38]. However, flaws in these generalized models are apparent. They receive no feedback from quarks and do not evolve with temperature or chemical potential, and they therefore do not meet the requirements of QCD in essence. A specific example is the first order chiral phase transition at low temperature and high density. There, the gluon propagators in the Nambu-Goldstone phase and in the Wigner phase should be different, and a discontinuous change is expected. In the face of this situation, the authors of [19,39] incorporate the quark's feedback into the gluon propagator by considering the contribution of quark loops in the gluon's DSE. Nevertheless, the quenched part of the gluon propagator relies on analyzing and fitting the lattice data.

In this paper, we will investigate an alternative treatment based on the operator product expansion (OPE), which provides an explicit form for the quark's feedback on gluon self-energy in terms of local quark condensates [40,41]. In this way, we derive a modified gluon propagator model and the consequent QCD phase diagram is studied within the DSE framework. Since the extraction of the quark's feedback on the gluon remains an open question, our model study will hopefully help us gain useful insights.

This paper is organized as follows. In Sec. II we introduce the quark gap equation and the truncation scheme. Then a gluon propagator model is derived from the gluon DSE with the help of the OPE. With this model, we study the transition behavior of QCD on the $T-\mu$ plane in remaining sections, where the case of $T=0$, $\mu\neq 0$ is discussed in Sec. III and $T\neq 0$, $\mu\neq 0$ is studied in Sec. IV. Finally, we summarize our results and give our conclusions in Sec. V.

II. QUARK GAP EQUATION AND GLUON PROPAGATOR MODEL

To study the QCD chiral phase transition, we employ the Dyson-Schwinger equation formalism, in which the quark gap equation at finite temperature and the chemical potential can be written as

$$[G(\vec{p},\tilde{\omega}_n)]^{-1}=[G^0(\vec{p},\tilde{\omega}_n)]^{-1}+T\sum_{l=-\infty}^{\infty}\int\frac{d^3q}{(2\pi)^3}\times\left[g^2D_{\mu\nu}(\vec{p}-\vec{q},\tilde{\omega}_n-\tilde{\omega}_l)\frac{\lambda^a}{2}\gamma_\mu G(\vec{q},\tilde{\omega}_l)\Gamma^a_\nu\right], \tag{1}$$

where the superscript 0 refers to free propagators. $\tilde{\omega}_n=(2n+1)\pi T+i\mu$ and the color index in gluon propagator $D_{\mu\nu}$ has been contracted. λ^a represents the Gell-Mann matrices and Γ^a_ν is the full quark-gluon vertex. Here, we have set all renormalization constants to one since we will use gluon models that are heavily suppressed in the ultraviolet region, rendering the integral in quark self-energy convergent. In this sense, the g^2 here is not a running coupling constant in the sense of the renormalization group but is rather an effective coupling, and therefore it has no medium dependence. We use Landau gauge here, which is a fixed point of the renormalization group and is therefore widely used in DSE studies [42]. The quark propagator can further be decomposed as

$$G^{-1}(\vec{p},\tilde{\omega}_n;T,\mu)=i\vec{\gamma}\cdot\vec{p}A(\vec{p}^2,\tilde{\omega}_n^2;T,\mu)+i\gamma_4\tilde{\omega}_nC(\vec{p}^2,\tilde{\omega}_n^2;T,\mu)+B(\vec{p}^2,\tilde{\omega}_n^2;T,\mu). \tag{2}$$

For the free quark propagator $G^0(\vec{p},\tilde{\omega}_n)$, scalar functions $A=1$, $B=m$, and $C=1$, where m is the current quark mass. Rainbow truncation has been popular in meson study because its combination with ladder truncation preserves the axial-vector Ward-Takahashi identity [43]. And in our case, as far as we know, no existing complicated vertices bring qualitative changes to the phase diagram. So, for simplicity, we will employ the rainbow truncation throughout this work, namely,

$$\Gamma^a_\nu(p,q)=\frac{\lambda^a}{2}\gamma_\nu. \tag{3}$$

In this way, we are left with the gluon propagator, which is undetermined. Generally, it can also be expressed through two scalar functions, D_T and D_L,

$$D_{\mu\nu}(\vec{k},\Omega_l)=P^T_{\mu\nu}(\vec{k},\Omega_l)D_T(\vec{k}^2,\Omega_l^2)+P^L_{\mu\nu}(\vec{k},\Omega_l)D_L(\vec{k}^2,\Omega_l^2), \tag{4}$$

with $P^L_{\mu\nu}$ and $P^T_{\mu\nu}$ being longitudinal and transverse projection operators, respectively,

$$P^T_{\mu\nu}(k)=(1-\delta_{\mu4})(1-\delta_{\nu4})\left(\delta_{\mu\nu}-\frac{k_\mu k_\nu}{\vec{k}^2}\right), \tag{5}$$

$$P^L_{\mu\nu}(k)=P_{\mu\nu}(k)-P^T_{\mu\nu}(k). \tag{6}$$

$\Omega_l=2l\pi T$ is the boson Matsubara frequency. Normally, one can now resort to the aforementioned models, e.g., the Qin-Chang model for D_T and D_L. However, since we are trying to incorporate the quark's feedback, further consideration is needed. Let us start with the case at zero temperature and density.

As we mentioned in Sec. I, extracting the quark's feedback from the gluon propagator is tricky. Inspired by the QCD sum rule [44], the authors of [41] suggested a relatively simple way, as follows. As we know, in the OPE

[1]Our work will be based on these bottom-up-scheme models which are determined by fitting hadron properties [35]. The other scheme, the top-down scheme, which aims to perform an *ab initio* computation of the gauge-sector DSEs, can be tracked in [36,37].

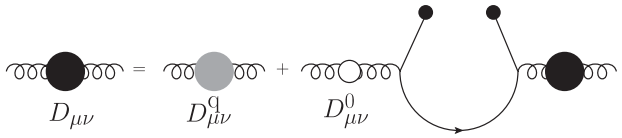

FIG. 1. Gluon DSE with a vacuum polarization term which contains a local quark condensate; see Eqs. (7) and (10).

framework, the current-current correlation function can be expressed through the various local scalar operators' vacuum expectation values, namely, vacuum condensates. These vacuum condensates characterizing the nonperturbative feature of QCD are treated as parameters in the QCD sum rules; they have been calculated elsewhere [45], including the DSEs [43,46]. For the gluon propagator, the gluon self-energy contains a quark condensate, which is the lowest dimension vacuum condensate generated by the quarks. The gluon vacuum polarization tensor involves the term [40,41]

$$\begin{aligned}\Pi^{\mathrm{Q}}_{\mu\nu}(k) &= -g^2 \int d^4(y-z) \int \frac{d^4q}{(2\pi)^4} e^{i(p-q)\cdot(y-z)} \\ &\quad \times \mathrm{tr}\left[\gamma_\mu \frac{1}{i\not{q}+m}\gamma_\nu \langle\bar{\psi}(y)\psi(z)\rangle\right] \\ &= P_{\mu\nu}(k) k^2 \Pi^{\mathrm{Q}}(k^2) \\ &= -P_{\mu\nu}(k)\frac{g^2 m\langle\bar{\psi}\psi\rangle}{3k^2} + \ldots, \end{aligned} \tag{7}$$

where $m\langle\bar{\psi}\psi\rangle = m_u\langle\bar{\psi}\psi\rangle_u + m_d\langle\bar{\psi}\psi\rangle_d$, and the ellipsis represents terms of higher order in m^2/k^2 which are neglected. The superscript Q stands for *quark*. Now, we can extract from the full gluon propagator a quark-unaffected part D^{q}, where q stands for *quenched*. Then the full gluon propagator is divided into two parts,

$$D_{\mu\nu}(k) = P_{\mu\nu} D(k^2) \tag{8}$$

$$= P_{\mu\nu}(D^{\mathrm{q}}(k^2) + D^{\mathrm{Q}}(k^2)). \tag{9}$$

Accordingly, with the DSE for the gluon propagator, we have

$$D_{\mu\nu}(k) = D^{\mathrm{q}}_{\mu\nu}(k) + D^{0}_{\mu\rho}(k)\Pi^{\mathrm{Q}}_{\rho\sigma}(k) D_{\sigma\nu}(k), \tag{10}$$

which is diagrammatically shown in Fig. 1. With Eqs. (7), (9), and (10), we have

$$\begin{aligned} D(k^2) &= \frac{D^{\mathrm{q}}(k^2)}{1+\frac{g^2 m\langle\bar{\psi}\psi\rangle_0}{3k^4}} \\ &\approx \frac{D^{\mathrm{q}}(k^2)}{1+\frac{\langle\bar{\psi}\psi\rangle_0}{\Lambda^3}}, \end{aligned} \tag{11}$$

where the subscript 0 refers to $T=0$ and $\mu=0$. Here, we introduce the momentum scale Λ as in [41], which absorbs the constants m, g and the momentum k and serves as a parameter in our model. With such simplification, the gluon propagator remains finite in the infrared region and the ultraviolet region will not be affected since $D^{\mathrm{q}}(k^2)$ will be heavily ultraviolet suppressed.

Then we extend Eq. (11) to finite temperature and chemical potential via $k \to k_l = (\vec{k}, \Omega_l)$ and $\langle\bar{\psi}\psi\rangle_0 \to \langle\bar{\psi}\psi\rangle_{T,\mu}$, so

$$D(\vec{k}^2 + \Omega_l^2) = \frac{D^{\mathrm{q}}(\vec{k}^2+\Omega_l^2)}{1+\frac{\langle\bar{\psi}\psi\rangle_{T,\mu}}{\Lambda^3}}. \tag{12}$$

Note that there is an implicit approximation $D_L = D_T$, which actually does not hold at finite temperature, as shown by lattice simulation [47,48]. However, for a sketchy study of the quark's feedback on the chiral phase diagram, we will continue to use this approximation, following earlier studies [18,38].

To specify the function $D^{\mathrm{q}}(k^2)$, we will employ the Qin-Chang model as the full gluon propagator at zero temperature and density,

$$g^2 D_{\mu\nu}(k^2) = \mathcal{G}(k^2) P_{\mu\nu} \tag{13}$$

$$\mathcal{G}(k^2) = \frac{8\pi^2}{\omega^4} D e^{-\frac{k^2}{\omega^2}}, \tag{14}$$

where the parameters D and ω are determined in hadron physics. D characterizes the interaction strength and ω controls the confinement length. In the rainbow-ladder truncation, the ground state pseudoscalar and the vector-meson observables, like the mass and the electroweak decay constant, are roughly constant while $Dw = (0.8\ \mathrm{GeV})^3$, with $\omega \in [0.4, 0.6]$ GeV. Therefore, the parameters are not completely constrained by hadron physics: a change in D can be compensated for by an alteration of ω. The Qin-Chang model qualitative agrees with modern DSEs and lattice studies in the gluon propagator's infrared region; e.g., it gives a typical value for the gluon screening mass [34].[2] So with Eqs. (8), (11), and (13), we have

$$D^q(k^2) = \frac{\mathcal{G}(k^2)}{g^2}\left(1+\frac{\langle\bar{\psi}\psi\rangle_0}{\Lambda^3}\right). \tag{16}$$

Substituting it into Eq. (12), we finally arrive at the OPE-modified model

[2]The Qin-Chang model improves upon a similar model, the Maris-Tandy model,

$$\mathcal{G}(k^2) = \frac{4\pi^2}{\omega^6} D k^2 e^{-\frac{k^2}{\omega^2}}, \tag{15}$$

in the deep-infrared region of the gluon propagator.

$$g^2 D(\vec{k}^2+\Omega_l^2) = \mathcal{G}(\vec{k}^2+\Omega_l^2)\frac{1+\frac{\langle\bar{\psi}\psi\rangle_0}{\Lambda^3}}{1+\frac{\langle\bar{\psi}\psi\rangle_{T,\mu}}{\Lambda^3}}. \quad (17)$$

Apparently, the form of $g^2D(\vec{k}^2+\Omega_l^2)$ changes as $\langle\bar{\psi}\psi\rangle$ evolves through the $T-\mu$ plane. At $T=0$ and $\mu=0$, it goes back to the Qin-Chang model; therefore, all hadron properties are preserved.

In the following calculation, we will choose $D=1.0\,\mathrm{GeV}^2$, $\omega=0.6\,\mathrm{GeV}$, and $m_u=m_d=0.005$ GeV in Eq. (14) for demonstration of almost all of the figures. As for the parameter Λ, from Eq. (17) we know that it characterizes the strength of the quark's feedback on the gluon: the larger that Λ is, the less the quark contributes. When $\Lambda\to+\infty$, Eq. (17) becomes

$$g^2D(\vec{k}^2+\Omega_l^2)\overset{\Lambda\to+\infty}{=}g^2D_s(\vec{k}^2+\Omega_l^2)=\mathcal{G}(\vec{k}^2+\Omega_l^2). \quad (18)$$

Here, we add a subscript s for *static* to this special case for later use. To determine Λ, we try to infer its value by comparing it with existing studies. For example, under rainbow truncation, [36] suggests about a 20% increase in $-\langle\bar{\psi}\psi\rangle_{\mathrm{u/d}}$ with the unquenching effect. In our case, we have $\langle\bar{\psi}\psi\rangle_{\mathrm{u/d}}=-(244\ \mathrm{MeV})^3$, obtained from $D_{\mu\nu}(k)$, compared with $\langle\bar{\psi}\psi\rangle^{\mathrm{q}}_{\mathrm{u/d}}=-(227\ \mathrm{MeV})^3$ from $D^{\mathrm{q}}_{\mu\nu}(k)$ by setting $\Lambda=0.56$ GeV.[3] We will show the responses of the CEP location and the pseudocritical line to these parameters at the end of Sec. IV.

III. PARTIAL RESTORATION OF CHIRAL SYMMETRY AT $T=0, \mu\neq 0$

The research on QCD at zero temperature and finite density is abundant and results in a lot of interest for researchers of cold QCD matter, e.g., compact stars [51,52]. For example, the equation of state of cold QCD matter plays an important role in calculating and understanding the structure and evolution of these stars [53–57]. There have also been studies suggesting a first order phase transition of chiral symmetry on the μ axis [58,59]. It is therefore interesting to see the picture from our model.

To solve the quark gap equation, we take the limit $T\to 0$. Then Eq. (1) becomes

$$[G(\vec{p},\tilde{p}_4)]^{-1}=[G^0(\vec{p},\tilde{p}_4)]^{-1}+\int\frac{d^4q}{(2\pi)^4}\times\left[g^2D_{\mu\nu}(\vec{p}-\vec{q},\tilde{p}_4-\tilde{q}_4)\frac{\lambda^a}{2}\gamma_\mu G(\vec{q},\tilde{q}_4)\Gamma^a_\nu\right], \quad (19)$$

where $\tilde{p}_4=p_4+i\mu$. Accordingly, the quark propagator can be decomposed as

$$G^{-1}(\vec{p},\tilde{p}_4;\mu)=i\vec{\gamma}\cdot\vec{p}A(\vec{p}^2,\tilde{p}_4;\mu)+i\gamma_4\tilde{p}_4C(\vec{p}^2,\tilde{p}_4;\mu)+B(\vec{p}^2,\tilde{p}_4;\mu). \quad (20)$$

We can also calculate the renormalized quark condensate with

$$\langle\bar{\psi}\psi\rangle=-\int\frac{dp^4}{(2\pi)^4}\mathrm{Tr}_{\mathrm{f,c,d}}[G(\vec{p},\tilde{p}_4;\mu)-G^0(\vec{p},\tilde{p}_4;\mu)]=-4N_cN_f\int\frac{dp^4}{(2\pi)^4}\frac{B}{A^2\vec{p}^2+C^2\tilde{p}_4{}^2+B^2}, \quad (21)$$

where the trace should be taken over flavor, color, and Dirac indices assuming the u, d quark symmetry.

Substitute Eqs. (17), (20), and (21) into Eq. (19), multiply both sides of Eq. (19) with $i\vec{\gamma}\cdot\vec{p}$, $i\gamma_4\tilde{p}_4$, and I_4, respectively, and then take the trace. One can obtain three coupled nonlinear equations of the functions A, B, and C. These nonlinear equations can be numerically solved with the iterative method. In this way, we can obtain the scalar functions A, B, C and the corresponding quark condensate.

Both the Nambu-Goldstone solution and the Wigner solution are found, corresponding to the Nambu-Goldstone phase and the Wigner phase, respectively. Figure 2 shows the $B(\vec{p}^2=0,p_4=0,i\mu)$ for both solutions and Fig. 3 displays the quark condensates. Both quantities are indicators of DCSB and exhibit a discontinuous drop at the same chemical potential.

One can notice from Fig. 3 that the $\langle\bar{\psi}\psi\rangle$ in the Nambu phase basically remains unchanged. This indicates that the partition function of QCD stays unchanged before μ reaches a critical value (roughly 1/3 of the baryon mass) [60]. Here, we would like to point out that this condition can be used as a rule in constraining gluon propagator

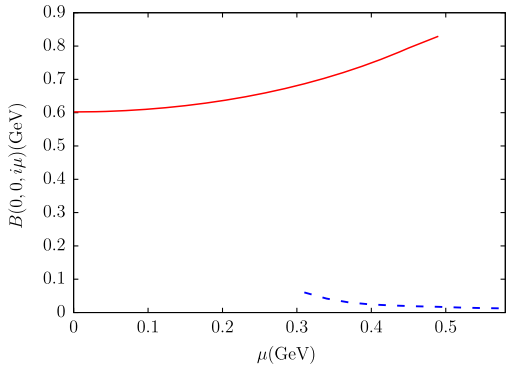

FIG. 2. Solution of the quark gap equation at zero temperature: $B(\vec{p}^2,p_4,i\mu)$ with $\vec{p}^2=0$, $p_4=0$. The two solutions correspond to the Nambu-Goldstone solution (the red solid curve) and the Wigner solution (the blue dashed curve), respectively.

[3] $-\langle\bar{\psi}\psi\rangle_{\mathrm{u/d}}=(244\ \mathrm{MeV})^3$ satisfies $-(m_u+m_d)\langle\bar{\psi}\psi\rangle_{\mathrm{u/d}}\approx m_\pi^2f_\pi^2$ (the Gell-Mann–Oakes–Renner relation [49]) within our parameter setting, although it is relatively small compared to the current lattice prediction $-\langle\bar{\psi}\psi\rangle_{\mathrm{u/d}}\approx(270\ \mathrm{MeV})^3$ [50].

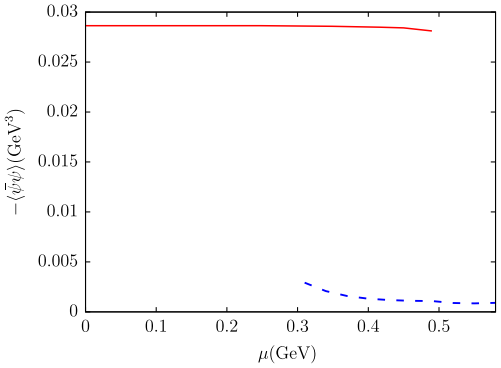

FIG. 3. Quark condenstate in the Nambu-Goldstone phase (the red solid curve) and the Wigner phase (the blue dashed curve).

models, which, however, was not satisfied at all times. For instance, in Refs. [21,61,62], a chemical-potential suppressed gluon propagator model is employed to study the QCD phase diagram, while $\langle\bar{\psi}\psi\rangle$ in that case actually varies with chemical potential and, therefore, breaks this rule to a certain extent. In our model here, this condition is satisfied because the whole quark's feedback is incorporated into a term solely described by quark condensate, which was already unchanged in the Nambu-Goldstone phase with static gluon models.

To study the possible phase transition between two phases, one should calculate the effective potential and obtain the pressure difference between them, whose zero point at μ_c is where the first order phase transition takes place. However, the Cornwall-Jackiw-Tomboulis effective potential action could only be used consistently with the rainbow truncation and a static gluon propagator model [63] and thus is invalid here. Nevertheless, suggested by other studies beyond the rainbow truncation, e.g., the Ball-Chiu vertex, first order phase transition should take place within the coexistence region of two solutions [18,64]. An intuitive guess for the first order phase transition point is [64]

$$\mu_c^{\chi} \approx \frac{\mu_c^{NG} + \mu_c^{W}}{2} = 0.4\ \mathrm{GeV}, \tag{22}$$

where μ_c^{NG} is where the Nambu-Goldstone solution disappears, while μ_c^{W} is where Wigner solution turns up. We would also like to point out that the μ_c^{W} from $D(k^2)$ is about 20 MeV lower than that from $D_s(k^2)$, indicating a small decrease in μ_c^{χ} within our model.

Finally, one could infer from Fig. 3 and Eq. (17) that our gluon propagator takes different forms in the Nambu-Goldstone phase and the Wigner phase, $D_{NG}(k^2) = D_s(k^2)$, compared with $D_W(k^2) \simeq D^q(k^2)$. Therefore, our gluon propagator has a clear distinction between the Nambu-Goldstone phase and the Wigner phase, which gives a solution to the problem we proposed in Sec. I. In this way, not only quark but also gluon propagators take discontinuous changes while the system goes through a first order phase transition. This gives a general picture about how the gluon propagator evolves at a finite μ, through the inclusion of the quark's feedback.

IV. PARTIAL RESTORATION OF CHIRAL SYMMETRY AT $T \neq 0$

We now move on to the finite temperature case and solve the gap equation at a finite T and μ. The quark condensate at finite temperature is

$$\langle\bar{\psi}\psi\rangle = -T\sum_{n=-\infty}^{+\infty}\int\frac{dp^3}{(2\pi)^3}\mathrm{Tr}_{\mathrm{f,c,d}}[G(\vec{p},\tilde{\omega}_n;T,\mu) - G^0(\vec{p},\tilde{\omega}_n;T,\mu)]. \tag{23}$$

Taking the limit $T \to 0$ in this equation leads to Eq. (21). Following similar steps as introduced in Sec. III (replace $\tilde{p}_4$ with $\tilde{\omega}_4$), we can again obtain the dressing functions and the corresponding quark condensate.

Let us first look at the results on the temperature axis, namely, $\mu = 0$. As we can see from Fig. 4, introducing the quark's feedback does not change the qualitative behavior of the quark condensate on the T axis. $\langle\bar{\psi}\psi\rangle$ is basically a monotonic decreasing function of T with an inflection point. If we use the susceptibility

$$\chi_T = \frac{\partial\langle\bar{\psi}\psi\rangle}{\partial T} \tag{24}$$

as the criterion [65,66], this inflection point is the so-called pseudocritical temperature. Another choice is the chiral susceptibility χ_m:

$$\chi_m = -\frac{\partial\langle\bar{\psi}\psi\rangle}{\partial m}. \tag{25}$$

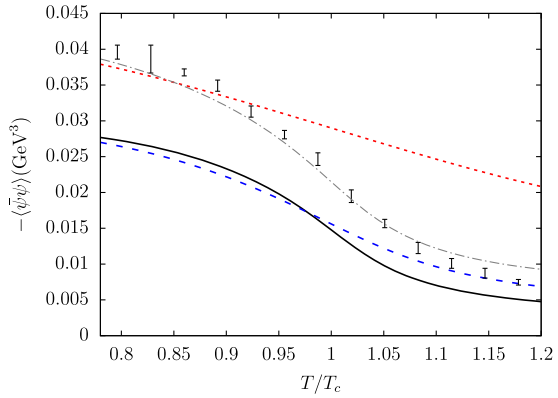

FIG. 4. Evolution of $\langle\bar{\psi}\psi\rangle$ at $T \neq 0$ and $\mu = 0$. $\langle\bar{\psi}\psi\rangle$ (the black solid curve) from our modified model Eq. (17) decreases faster than $\langle\bar{\psi}\psi\rangle_s$ (blue dashed curve) from the static model equation (18). The other $\langle\bar{\psi}\psi\rangle$ (the gray dot-dashed curve) and $\langle\bar{\psi}\psi\rangle_s$ (the red dotted curve) were obtained by setting the parameter $D = 1.4$ and $\Lambda = 0.62$, whose choice is explained in the text. The data (the black error bars) are taken from the lattice calculation [8].

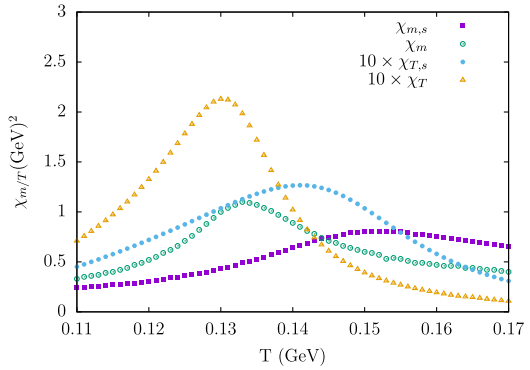

FIG. 5. Susceptibilities at finite temperature and zero chemical potential. χ_T and χ_m are defined in Eqs. (24) and (25) with the subscript s for *static*.

The maxima of χ_T and χ_m, namely, the pseudocritical temperatures—the T_c's—do not necessarily coincide with each other [67], although within our model they are closer (see Fig. 5). Nevertheless, all of these susceptibilities exhibit smooth change; hence, it is a crossover in this area.

However, some quantitative changes are noticeable. In Fig. 5, the T_c's from the two gluon propagator models are not the same: $D(k^2)$ gives a relatively low T_c. This can be understood with the help of Fig. 4: when T goes up, $-\langle\bar{\psi}\psi\rangle$ drops continuously, so $D(k^2)$ gets smaller and leads to a weakening of the interaction between the quarks. This then, in turn, accelerates the dropping of the quark condensate, producing relatively low T_c's. Compared with that of the static gluon model, this "quicker" transition brought by the quark's feedback is closer to the lattice result concerning the slopes of the $\langle\bar{\psi}\psi\rangle$ curves near the T_c. We notice that the $\langle\bar{\psi}\psi\rangle$ and the T_c's we give are relatively low compared to the lattice predictions $T_c \approx 160$ MeV and $\langle\bar{\psi}\psi\rangle_{\mathrm{u/d}} \approx -(280\ \mathrm{MeV})^3$ given in [8]. This is due to our simplified truncation scheme and gluon model. In order to perform a direct comparison with the lattice result, we primitively raise the interaction strength to $D = 1.4$ and $\Lambda = 0.62$ (the choice of Λ is explained in the caption of Table I), which produces $\langle\bar{\psi}\psi\rangle_{\mathrm{u/d}} = -(277\ \mathrm{MeV})^3$. The $\langle\bar{\psi}\psi\rangle_T$ still agrees with lattice data better than a static model, as shown in Fig. 4. Therefore, we conclude that our modified model persists to give more realistic descriptions of transition behavior at the finite temperature $T \leq T_c$.

It is worth noting that, in contrast to that on the μ axis where $D(k^2)$ takes a sudden change, here $D(k^2)$ decreases continuously. Such behavior is naturally generated in our model and qualitatively agrees with the lattice result on $D_T(k^2)$ [68].

With the results on the μ axis and the T axis, we are led to believe transition behaviors like crossover and first order phase transition will remain on the $T-\mu$ plane, while the transition lines will somehow vary. Consequently, the CEP, which is the end point of the first order phase transition line, may shift.

$\langle\bar{\psi}\psi\rangle$ at $T \neq 0$ and $\mu \neq 0$ are shown in Fig. 6, where $\langle\bar{\psi}\psi\rangle$ undergoes continuous change with a low μ, while exhibiting a discontinuous transition with a larger μ. Figure 7 shows that the corresponding susceptibilities display different behaviors, e.g., at $\mu = 110$ MeV and $\mu = 80$ MeV they are continuous, while at $\mu = 130$ MeV they

TABLE I. Parameter dependence of the CEP location and curvature parameter κ defined in Eq. (26). In row 4 and row 5, Λ is determined by the same criterion as in row 2: $\langle\bar{\psi}\psi\rangle_0^{\mathrm{q}}/\langle\bar{\psi}\psi\rangle_0 = 0.8$.

D	ω	Λ (GeV)	T_c (GeV)	$(T_E,\mu_E)/T_c$	κ
1.0	0.6	0.5	0.125	(0.89,1.01)	0.116
1.0	0.6	0.56	0.131	(0.85,1.11)	0.126
1.0	0.6	$+\infty$	0.141	(0.82,1.13)	0.143
1.0	0.5	0.52	0.156	(0.93,0.41)	0.333
1.4	0.6	0.62	0.176	(0.93,0.46)	0.323

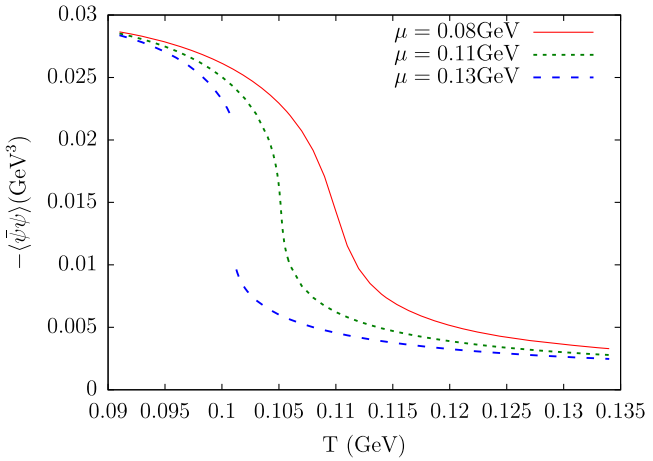

FIG. 6. $\langle\bar{\psi}\psi\rangle$ at finite μ and T.

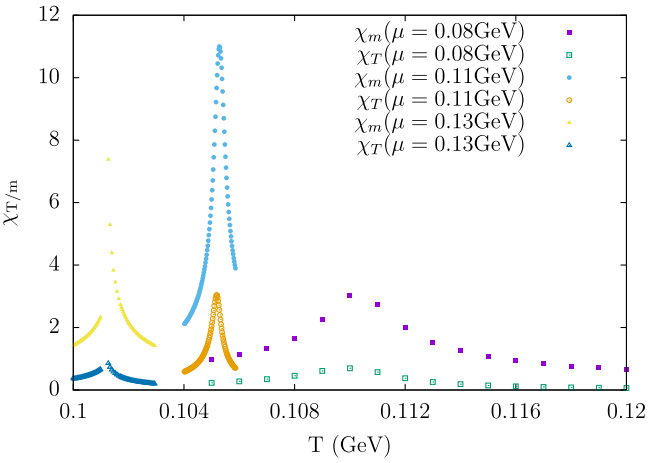

FIG. 7. Crossover and first order phase transition characterized by susceptibilities. The peaks go to infinity, approaching the critical end point.

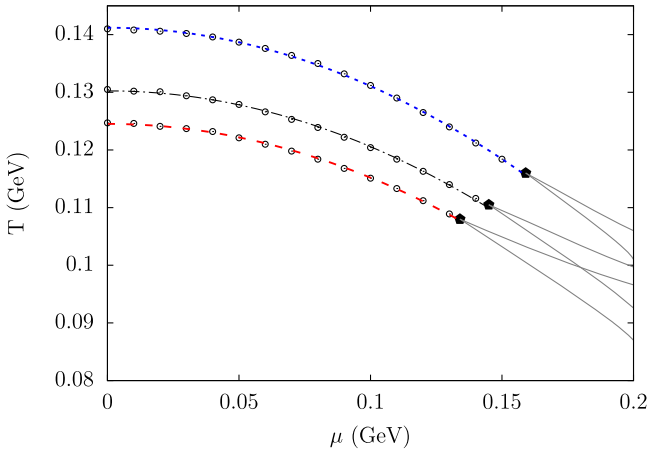

FIG. 8. From top to bottom, pseudotransition points obtained from $\Lambda = +\infty$ (the blue dotted curve) $\Lambda = 0.56$ (the black dot-dashed line), and $\Lambda = 0.5$ (the red dashed curve), respectively, are all well fitted by Eq. (26). The area between the gray solid curves is the metastable region of the Nambu-Goldstone phase and the Wigner phase.

are not. One could also see there is a tendency for the susceptibilities to diverge at some point when μ is larger than 110 MeV. This point is then the second order phase transition point, namely, the CEP.

We therefore determine the pseudocritical lines in Fig. 8 by taking the maxima of χ_T. For comparison, again we also add the result of $D_s(k^2)$. It shows, with the quark's feedback on the gluon propagator, the pseudocritical line gets flattened. This can be seen more clearly with the parametrization formula [12,69]:

$$T_c(\mu) = T_c(0)[1 - \kappa\mu^2/T_c^2(0) + O(\mu^4/T_c^4(0))], \quad (26)$$

where $T_c(\mu)$ parametrizes the pseudotransition line. We extract κ by least-squares fit and plot the functions $T_c(\mu)$ in Fig. 8. The root-mean-square deviation in this fitting,

$$\mathrm{RMSD} = \sqrt{\frac{1}{N}\sum_{i=1}^{N}(T_c(\mu_i) - T_c^i)^2}, \quad (27)$$

is RMSD < 0.2 MeV for all curves.

The first three rows in Table I show κ's from different Λ's, along with the T_c's and the CEP locations in Fig. 8. We can see that there is a consistent decrease in κ and an increase in T_E/T_c as Λ decreases. The same conclusion can be drawn when we employ the Maris-Tandy model, namely, Eq. (15), for which the calculation will not be detailed here. Note that lattice QCD suggests that $\kappa \approx 0.05$–0.06 [11,12,69] and estimates $(T_E, \mu_E)/T_c \approx (0.9$–$0.95, 1.0$–$1.4)$ [70]. Given that, in general, model studies tend to give a relatively large κ and a low T_E/T_c [71], our model therefore provides a means for improvement in these cases.

In the last two rows of Table I, the response of the CEP's location to varying the parameters D and ω, respectively, is shown. As explained at the end of [18], if we consider $r = 1/\omega$ as a confinement length scale, then when r goes to zero, which represents a NJL-type model, the CEP would rotate toward the chemical-potential axis. Therefore, the CEP rotates toward the temperature axis from row 2 to row 4. In row 5, the interaction strength D is raised to produce a larger $-\langle\bar{\psi}\psi\rangle_{\mathrm{u/d}} \approx (280\ \mathrm{MeV})^3$, which corresponds to the gray dot-dashed curve in Fig. 4. The CEP in this case also rotates toward the temperature axis. So, generally speaking, reducing ω would make the CEP rotate toward the temperature axis under the constraint of $D\omega \approx (0.8\ \mathrm{GeV})^3$.

V. DISCUSSION AND SUMMARY

To summarize, we incorporate the quark's feedback into the gluon propagator based on the idea of the OPE and derive a gluon propagator that evolves through the $T - \mu$ plane. It is characterized and determined by a quark condensate at finite temperature and density. The QCD phase diagram is then studied with this gluon model within the DSE framework.

At zero temperature and finite chemical potential, the coexistence region of the Nambu-Goldstone solution and the Wigner solution is found, indicating a first order phase transition point. Moreover, we have shown that our model preserves two important features of QCD; e.g., QCD remains vacuum at low chemical potential and discontinuous change in the gluon propagator at the first order phase transition. Then we move on to $T \neq 0$ case and find that the quark's feedback accelerates the decrease of quark condensate, leading to a quicker crossover on the temperature axis. Such a picture agrees with the lattice simulation at finite temperature. We further studied the crossover region and the CEP location. It shows a consistent decrease in curvature parameter κ and an increase in T_E/T_c, with more of a gluon propagator distributed to the quark's feedback. For example, it brings a CEP location from $(T_E, \mu_E)/T_c = (0.82, 1.13)$ to $(T_E, \mu_E)/T_c = (0.85, 1.11)$ and κ from 0.143 to 0.126, both closer to the lattice estimation. We therefore believe our scheme could provide a means for improvement in model studies which have not considered the quark's feedback.

Finally, it is worth noting that this work is a supplement to existing investigations of refined quark-gluon vertices beyond rainbow truncation. The authors of [18] have shown that with the Ball-Chiu vertex, the QCD phase diagram is improved in several aspects; e.g., it has a significantly narrower metastable region and a more reasonable CEP location. Since the dressing effect in the Ball-Chiu vertex is also expressed in terms of the quark's dressing functions and therefore consists of the quark's feedback, it is evident that the incorporation of the quark's feedback within the DSE framework could produce a QCD phase diagram that is more realistic.

ACKNOWLEDGMENTS

We benefited from a discussion with Fei Gao and thank him for providing valuable insights. This work is supported in part by the National Natural Science Foundation of China (under Grants No. 11275097, No. 11475085, No. 11265017, and No. 11247219), the National Basic Research Program of China (under Grant No. 2012CB921504), the Jiangsu Planned Projects for Postdoctoral Research Funds (under Grant No. 1402006C), the National Natural Science Foundation of Jiangsu Province of China (under Grant No. BK20130078), and Guizhou province outstanding youth science and technology talent cultivation object special funds [under Grant No. QKHRZ(2013)28].

[1] J. Adams *et al.* (STAR Collaboration), Nucl. Phys. **A757**, 102 (2005).
[2] E. Shuryak, Prog. Part. Nucl. Phys. **62**, 48 (2009).
[3] E. Shuryak, Prog. Part. Nucl. Phys. **53**, 273 (2004).
[4] W. Zajc, Nucl. Phys. **A805**, 283 (2008).
[5] G. Odyniec, EPJ Web Conf. **95**, 03027 (2015).
[6] D. McDonald (STAR Collaboration), EPJ Web Conf. **95**, 01009 (2015).
[7] A. Bazavov, T. Bhattacharya, M. Cheng, C. DeTar, H. Ding *et al.*, Phys. Rev. D **85**, 054503 (2012).
[8] S. Borsanyi, Z. Fodor, C. Hoelbling, S. D. Katz, S. Krieg, C. Ratti, and K. K. Szabo (Wuppertal-Budapest Collaboration), J. High Energy Phys. 09 (2010) 073.
[9] A. Bazavov *et al.* (HotQCD Collaboration), Phys. Rev. D **90**, 094503 (2014).
[10] M. Troyer and U.-J. Wiese, Phys. Rev. Lett. **94**, 170201 (2005).
[11] P. de Forcrand and O. Philipsen, Phys. Rev. Lett. **105**, 152001 (2010).
[12] G. Endrodi, Z. Fodor, S. Katz, and K. Szabo, J. High Energy Phys. 04 (2011) 001.
[13] P. Costa, M. Ruivo, and C. de Sousa, Phys. Rev. D **77**, 096001 (2008).
[14] P. Costa, C. de Sousa, M. Ruivo, and H. Hansen, Europhys. Lett. **86**, 31001 (2009).
[15] D. Nickel, Phys. Rev. D **80**, 074025 (2009).
[16] V. Skokov, B. Friman, and K. Redlich, Phys. Rev. C **83**, 054904 (2011).
[17] A. Ayala, A. Bashir, J. Cobos-Martinez, S. Hernandez-Ortiz, and A. Raya, Nucl. Phys. **B897**, 77 (2015).
[18] S.-x. Qin, L. Chang, H. Chen, Y.-x. Liu, and C. D. Roberts, Phys. Rev. Lett. **106**, 172301 (2011).
[19] C. S. Fischer and J. Luecker, Phys. Lett. B **718**, 1036 (2013).
[20] X.-y. Xin, S.-x. Qin, and Y.-x. Liu, Phys. Rev. D **90**, 076006 (2014).
[21] C. Shi, Y.-L. Wang, Y. Jiang, Z.-F. Cui, and H.-S. Zong, J. High Energy Phys. 07 (2014) 014.
[22] W. Weise, Prog. Part. Nucl. Phys. **67**, 299 (2012).
[23] A. Bashir, L. Chang, I. C. Cloet, B. El-Bennich, Y.-X. Liu, C. D. Roberts, and P. C. Tandy, Commun. Theor. Phys. **58**, 79 (2012).
[24] F. Gao, S.-X. Qin, Y.-X. Liu, C. D. Roberts, and S. M. Schmidt, Phys. Rev. D **89**, 076009 (2014).
[25] F. Gao, J. Chen, Y.-X. Liu, S.-X. Qin, C. D. Roberts, and S. M. Schmidt, arXiv:1507.00875.
[26] D. Müller, M. Buballa, and J. Wambach, Eur. Phys. J. A **49**, 96 (2013).
[27] S.-S. Xu, Z.-F. Cui, B. Wang, Y.-M. Shi, Y.-C. Yang, and H.-S. Zong, Phys. Rev. D **91**, 056003 (2015).
[28] B. Wang, Y.-L. Wang, Z.-F. Cui, and H.-S. Zong, Phys. Rev. D **91**, 034017 (2015).
[29] J. S. Ball and T.-W. Chiu, Phys. Rev. D **22**, 2542 (1980).
[30] C. S. Fischer, Phys. Rev. Lett. **103**, 052003 (2009).
[31] C. Burden, L. Qian, C. D. Roberts, P. Tandy, and M. J. Thomson, Phys. Rev. C **55**, 2649 (1997).
[32] D. Blaschke, G. Burau, Y. Kalinovsky, P. Maris, and P. Tandy, Int. J. Mod. Phys. A **16**, 2267 (2001).
[33] P. Maris and P. C. Tandy, Phys. Rev. C **60**, 055214 (1999).
[34] S.-x. Qin, L. Chang, Y.-x. Liu, C. D. Roberts, and D. J. Wilson, Phys. Rev. C **84**, 042202 (2011).
[35] D. Binosi, L. Chang, J. Papavassiliou, and C. D. Roberts, Phys. Lett. B **742**, 183 (2015).
[36] C. S. Fischer and R. Alkofer, Phys. Rev. D **67**, 094020 (2003).
[37] A. C. Aguilar, D. Binosi, and J. Papavassiliou, Phys. Rev. D **78**, 025010 (2008).
[38] M. He, F. Hu, W.-M. Sun, and H.-S. Zong, Phys. Lett. B **675**, 32 (2009).
[39] C. S. Fischer, J. Luecker, and J. A. Mueller, Phys. Lett. B **702**, 438 (2011).
[40] T. G. Steele, Z. Phys. C **42**, 499 (1989).
[41] Y. Jiang, H. Gong, W.-m. Sun, and H.-s. Zong, Phys. Rev. D **85**, 034031 (2012).
[42] C. D. Roberts and S. M. Schmidt, Prog. Part. Nucl. Phys. **45**, S1 (2000).
[43] P. Maris and C. D. Roberts, Phys. Rev. C **56**, 3369 (1997).
[44] M. A. Shifman, Prog. Theor. Phys. Suppl. **131**, 1 (1998).
[45] C. McNeile, A. Bazavov, C. T. Davies, R. J. Dowdall, K. Hornbostel, G. P. Lepage, and H. D. Trottier, Phys. Rev. D **87**, 034503 (2013).
[46] H.-s. Zong, J.-l. Ping, H.-t. Yang, X.-f. Lu, and F. Wang, Phys. Rev. D **67**, 074004 (2003).
[47] A. Cucchieri, A. Maas, and T. Mendes, Phys. Rev. D **75**, 076003 (2007).
[48] P. J. Silva, O. Oliveira, P. Bicudo, and N. Cardoso, Phys. Rev. D **89**, 074503 (2014).
[49] M. Gell-Mann, R. J. Oakes, and B. Renner, Phys. Rev. **175**, 2195 (1968).
[50] S. Aoki *et al.*, Eur. Phys. J. C **74**, 2890 (2014).

[51] M. Alford, D. Blaschke, A. Drago, T. Klahn, G. Pagliara, and J. Schaffner-Bielich, Nature (London) **445**, E7 (2007).
[52] S. Weissenborn, I. Sagert, G. Pagliara, M. Hempel, and J. Schaffner-Bielich, Astrophys. J. **740**, L14 (2011).
[53] M. Buballa, Phys. Rep. **407**, 205 (2005).
[54] J. O. Andersen and M. Strickland, Phys. Rev. D **66**, 105001 (2002).
[55] H. Chen, M. Baldo, G. Burgio, and H.-J. Schulze, Phys. Rev. D **86**, 045006 (2012).
[56] H. Li, X.-L. Luo, and H.-S. Zong, Phys. Rev. D **82**, 065017 (2010).
[57] T. Zhao, S.-S. Xu, Y. Yan, X.-L. Luo, X.-J. Liu, and H.-S. Zong, Phys. Rev. D **92**, 054012 (2015).
[58] M. Asakawa and K. Yazaki, Nucl. Phys. **A504**, 668 (1989).
[59] T. Hell, K. Kashiwa, and W. Weise, Phys. Rev. D **83**, 114008 (2011).
[60] A. M. Halasz, A. Jackson, R. Shrock, M. A. Stephanov, and J. Verbaarschot, Phys. Rev. D **58**, 096007 (1998).
[61] H. Chen, M. Baldo, G. F. Burgio, and H. J. Schulze, Phys. Rev. D **84**, 105023 (2011).
[62] Y. Jiang, H. Chen, W.-M. Sun, and H.-S. Zong, J. High Energy Phys. 04 (2013) 014.
[63] J. M. Cornwall, R. Jackiw, and E. Tomboulis, Phys. Rev. D **10**, 2428 (1974).
[64] H. Chen, W. Yuan, L. Chang, Y.-X. Liu, T. Klahn, and C. D. Roberts, Phys. Rev. D **78**, 116015 (2008).
[65] K. Morita, V. Skokov, B. Friman, and K. Redlich, Phys. Rev. D **84**, 074020 (2011).
[66] V. Skokov, Phys. Rev. D **85**, 034026 (2012).
[67] Y.-l. Du, Z.-f. Cui, Y.-h. Xia, and H.-s. Zong, Phys. Rev. D **88**, 114019 (2013).
[68] C. S. Fischer, A. Maas, and J. A. Muller, Eur. Phys. J. C **68**, 165 (2010).
[69] O. Kaczmarek, F. Karsch, E. Laermann, C. Miao, S. Mukherjee, P. Petreczky, C. Schmidt, W. Soeldner, and W. Unger, Phys. Rev. D **83**, 014504 (2011).
[70] S. Sharma, Adv. High Energy Phys. (Cairo, Egypt) **2013**, 452978 (2013).
[71] M. A. Stephanov, QCD phase diagram: An overview, *Proc. Sci.*, LAT2006 (2006) 024 [arXiv:hep-lat/0701002].